2013 International Conference on Unmanned Aircraft Systems (ICUAS)
May 28-31, 2013, Grand Hyatt Atlanta, Atlanta, GA

A HIL Testbed for Small Unmanned Helicopter's Initial Controller Gain Tuning

Sepehr P. Khaligh[1], Alejandro Martínez[2], Farbod Fahimi[3] and Charles Robert Koch[4]

Abstract— **A Hardware-In-The-Loop (HIL) testbed design for small unmanned helicopters is described. The testbed provides a safe and low-cost platform to implement control algorithms and tune the control gains in a controlled environment. Specifically, it allows for testing the robustness of the controller to external disturbances by emulating the hover condition. A 6-DOF nonlinear mathematical model of the helicopter has been validated in real flight tests. This model is implemented in real-time to estimates the states of the helicopter which are then used to determine the actual control signals on the testbed. A damping system with a negligible parasitic effect on the dynamics of the helicopter around hover is incorporated into the testbed design to minimize the structural stress on the fuselage in the case of controller failure or a subsystem malfunction. Three experiments including the longitudinal, lateral and heading control tests are performed. Experimental results show that the HIL testbed allows for designing a controller which is robust to the external disturbances, and achieves an accuracy of $\pm 2cm$ in the position control along the longitudinal and lateral axes in hover, and that of $\pm 1deg$ around the yaw axis on the heading trajectory tracking.**

I. INTRODUCTION

Unmanned aerial systems have recently received growing attention due to their broad range of applications [1]–[5]. Researchers are working on different types and sizes of Unmanned Aerial Vehicle (UAV) platforms, from Micro-Air-Vehicles (MAV) including Quadrotors and micro fixed-wing aircrafts, to Ultra-High-Endurance (UHE) vehicles [6]–[12]. During the process from conceptual design to fabrication and deployment, a number of technical and theoretical challenges must be solved. UAV control is a challenging multidisciplinary problem that combines control with aerodynamics. Particularly challenging are the platforms of Vertical Take-off and Landing (VTOL), among which unmanned helicopters are one of the most demanding ones.

Due to their inherent instability, model nonlinearity, non-minimum phase behavior, and aerodynamic complexity, unmanned helicopters offer tremendous challenges during the control design and implementation phases [13]–[18]. In-flight tuning of control parameters of small unmanned helicopters is difficult due to their high manoeuvrability and inherent instability properties, and catastrophic damage in the event of a crash. Although, computer simulation is extremely useful to test controller performance, an intermediate step between simulation and real flight test allows for implementation issues on the real hardware to be tested.

From simple testbed configurations to complete and costly Hardware-In-The-Loop (HIL) simulation testbeds, a variety of systems have been reported in the literature. A 3-DOF testbed for quadrotor attitude stabilization is described in [19] and it consists of a single pole fixed to the ground at one end and a spherical joint allowing 3-DOF about the Euler angles at the other end. The quadrotor is then stabilized by implementing a robust fuzzy controller. The single pole structure is simple and affordable, but it may not be suitable for larger helicopters which are capable of generating considerable lift and moments.

Another approach is presented in [20] and [21] for a 3-DOF motion control of a setup [22]. This system consists of an arm with a platform on one end and two propellers mounted to the platform to emulate a helicopter. The platform itself has 1-DOF motion about pitch axis and the whole arm is balanced with a counterweight at the other end. Thus the arm is free to move in both elevation and azimuthal directions. In addition, the main arm is equipped with a motorized lead screw, allowing the motion of a mass attached to it. In this way, controllable and quantifiable disturbances can be generated. This setup is useful to study nonlinearities, uncertainties, unmodeled dynamics, etc. as in [20] where adaptive output feedback control is used to reject parameter uncertainties and unmodeled dynamics including actuator saturation. Similarly, [21] proposed an adaptive controller to reject nonlinearities and unmodeled dynamics and in order to provide a robust control solution. However, due to the constraints imposed by this system, it does not represent the response of an actual helicopter. For example, the emulated helicopter cannot perform a free translational motion and its Center of Gravity (CG) is constrained to the surface of a sphere.

To test the landing phase in difficult terrains for helicopters, a 5-DOF HIL testbed is developed in [23]. Here, the system is composed of a 5-DOF test platform, a computer that controls the motion of the testbed, and an avionics box. The testbed itself can perform linear absolute motion about x, y and z axis, and two angular motion, pan and tilt, to the platform in which the helicopter's avionics is attached. Therefore, the testbed in conjunction with the avionics box are used to emulate the helicopter's motion based on the dynamic model, providing a high repeatability on emulated

[1]S. P. Khaligh is with the Department of Mechanical Engineering, University of Alberta, Edmonton, AB T6G 2G8, Canada sepehr.khaligh@ualberta.ca

[2]A. Martinez is with the Department of Mechanical Engineering, University of Alberta, Edmonton, AB T6G 2G8, Canada ma39@ualberta.ca

[3]F. Fahimi is with Faculty of Mechanical and Aerospace Engineering, The University of Alabama in Huntsville, Huntsville, AL 35899, USA fahimi@eng.uah.edu

[4]C. R. Koch is with Faculty of Mechanical Engineering, University of Alberta, Edmonton, AB T6G 2G8, Canada bob.koch@ualberta.ca

flight trajectory tracking in a controlled environment. Although, this is an effective solution to the problem of landing on difficult terrains, it is not adequate for those cases in which unmodeled dynamics or unexpected disturbance of the helicopter are present, since the actual helicopter is not included.

Another approach that involves a 5-DOF testbed, is presented in [24]. The setup is a customized version of the Whitman [25]. It is composed of a central shaft with an arm attached to it, which allows azimuthal and elevation motion. At the end of the arm there is a platform allowing rotation in the three Euler directions. The helicopter cannot perform a free translational motion but constrained motion is allowed by the testbed. A fuzzy logic based algorithm is used to control the helicopter on the testbed. Although the testbed works well with the fuzzy logic control as a non model-based algorithm, it is difficult to use this testbed for model-based control. This is due to the constraints imposed by the testbed on the translational motion of the helicopter which modifies the real unconstrained helicopter response. For example, to increase the altitude of the helicopter on the testbed, its center of gravity (CG) must move towards the center of the testbed, and CG is constrained to the surface of a sphere and cannot move freely in space.

A 6-DOF indoor stand is presented in [26] for control studies. The testbed is composed of a linkage mechanism that allows for the free motion of the helicopter in a $2m$ cube. The symmetrical geometry of the mechanism makes it equivalent to a concentrated mass, and the design of the stand allows for the free 6-DOF motion of the helicopter. However, the mechanism attached to the helicopter constantly alters the 3D location of its CG during the operation, and the added dynamics of the testbed might not be negligible.

Another approach is presented in [27] to test the performance of MAVs in near-Earth environments such as forests or in an urban environment. The design concept is a 6-DOF gantry attached to a non-flying mockup of a MAV. The mockup emulates the motion of the MAV using a high-fidelity mathematical model and a control system that moves the gantry accordingly. The test rig is especially equipped for emulating adverse weather conditions such as fog, rain and dust. Although, the concept provides a suitable solution for testing MAVs in the Near-Earth environments, it might not be suitable for the cases dealing with unmodeled dynamics, since the actual vehicle is not included.

To facilitate tuning of control gains as well as testing both model-based and non-model-based controllers against external disturbances for small unmanned helicopters, a low-cost Hardware-In-The-Loop (HIL) testbed is designed, built, and tested. By implementing the 6-DOF nonlinear mathematical model of the helicopter, the developed HIL simulation generates the actual motion of the vehicle and calculates the states. Then, an onboard microcomputer determines the control signals to the actual helicopter mounted on the testbed. A 2-DOF testbed setup configurable for individually testing the longitudinal, lateral, and heading control is presented. A special damping system is designed to emulate the hover maneuver. It exerts no damping in hover, which allows for the hover control testing without any interference from the damping system. If the helicopter deviates from its nominal hover position, the damping increases and smoothly slows down the motion. This minimizes the structural stress on the fuselage and rotor mechanism.

The remainder of the paper is organized into sections. Section II describes the architecture of the HIL simulation testbed design. In section III, the testbed modeling is described. The control design is presented in section IV. Finally, the experimental results from the longitudinal, lateral, and heading tests are presented in Section V, and the paper concludes in section VI.

II. HARDWARE-IN-THE-LOOP (HIL) SIMULATION

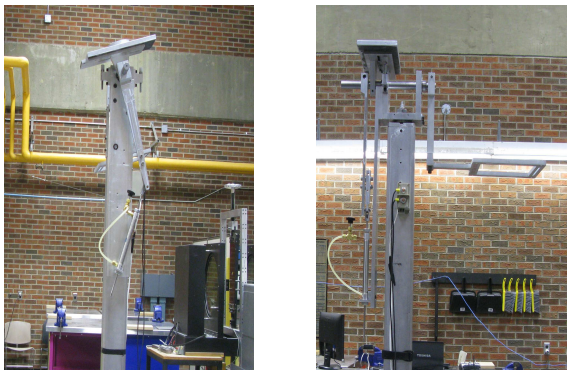

Fig. 1. Front and side views of the HIL testbed

Controller gain tuning is often part of a control design, and requires the system to be in operation during the tuning process. For small unmanned helicopters, in-flight gain tuning is potentially risky and expensive due to the high manoeuvrability and internal instability properties of these vehicles which may result in catastrophic equipment failure during the tuning process. In order to facilitate safe tuning of control gains as well as testing a controller against external disturbances in a controlled environment, a Hardware-In-The-Loop (HIL) testbed design for small unmanned helicopters has been developed and is shown in Fig. 1.

Schematics of the testbed from the front and side views are shown in Fig. 2. This testbed is a 2-DOF system composed of a long pole to raise the helicopter off the floor to eliminate the ground effect, and a headpiece. The pole is anchored to the ground, and the headpiece is connected to the pole through a set of thrust roller bearings, which allows for the rotation of the head with respect to the pole around the vertical Z-axis. The headpiece itself is composed of: a U-shape aluminum plate, two arms, a damping cylinder, a counter balance weight, and one stopper on each side. The helicopter is mounted on Arm 1 which is connected to arm 2 through two ball bearings on the U-shape plate. This allows for the rotation of the helicopter around the horizontal X-axis. To individually test the longitudinal/lateral motion, a mechanical device restricts the rotation of the headpiece

around the vertical axis. Two adjustable hard stoppers restrict the rotation around the X-axis to $\pm 30deg$. In the event of controller malfunction, a nonlinear passive damping system, shown on the front view in Fig. 2, prevents the helicopter from hitting the hard stoppers at a large angular speed.

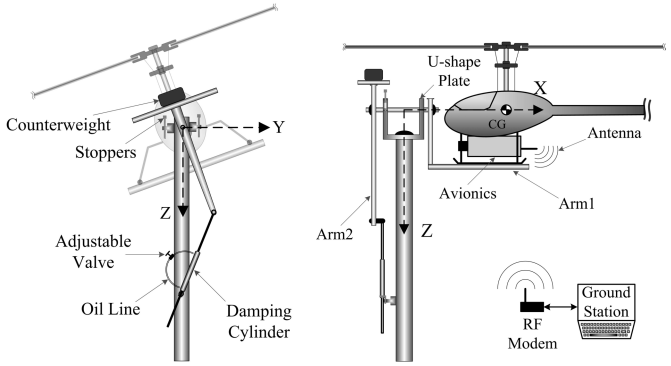

Fig. 2. HIL Testbed schematics, front and side views

The damping system is composed of a double acting cylinder, fully filled with a light oil NUTO A10. An oil line with an adjustable needle valve connects the cylinder's inlet to its outlet and makes a closed path of oil. Since the cylinder is double acting and its rod extends from both ends of the barrel, it allows for the continuous flow of oil between the chambers and does not require any oil reservoir.

When testing the helicopter around hover on the testbed, the cylinder is vertical and creates a negligible damping due to the vertical mechanism geometry. As the helicopter deviates from hover, the cylinder angle relative to the vertical pole increases and the damping increases in a nonlinear manner. Once the control gains are properly tuned for hover, the damping cylinder is removed and the controller is tested against external disturbances.

The counter weight is chosen to precisely balance the arms to mimic hover condition, and the mechanism shown in Fig. 2 is designed such that the CG of the helicopter is aligned with the horizontal X-axis which is the axis of rotation in roll and pitch tests.

The goal of the designed HIL simulation testbed is to test the longitudinal, lateral and heading controller of the helicopter in real-time on the ground. The testbed provides a safe and low-cost mean to implement a control algorithm and tune the control gains. Specifically, it allows for testing the robustness of the controller against external disturbances. Using this testbed, the helicopter can be disturbed manually or mechanically during the operation and the performance of the controller can be improved. This is difficult to do in a real flight test. Furthermore, the testbed is designed such that the added dynamics due to the testbed itself is negligible. The testbed can also be used for testing the avionics of small helicopters on the ground. The disadvantage of this HIL system is that all degrees of freedom cannot be tested simultaneously, and they must be tested one at a time.

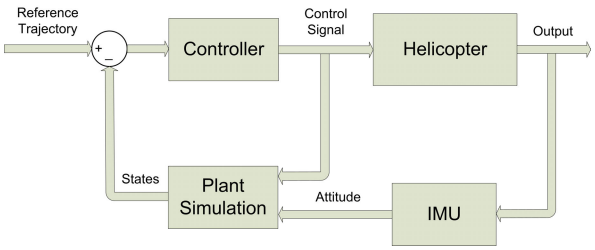

Fig. 3. Block diagram of the HIL simulation

The block diagram of the HIL simulation is shown in Fig. 3. The Controller block represents the onboard embedded control system which calculates and outputs control signals to the actual servos of the helicopter. The Helicopter represents the physical helicopter to be tested. The IMU block represents the Inertial Measurement Unit, which determines the actual attitude of the helicopter including the Euler angles and their rates at every sampling time. However, as the helicopter is fixed on the testbed, its position and velocity are determined using the plant simulation model. The Plant Simulation generates the actual motion of the helicopter using its 6-DOF nonlinear mathematical model. It receives the control signals calculated by the controller, along with the current IMU outputs, and determines the position and velocity of the simulated helicopter at every sampling time by integrating from the 6-DOF equations of motion. The calculated states of the helicopter are then used as the feedback signal to the controller for the next sampling time computations. This HIL is implemented in real-time at a sample rate of $50Hz$ using xPC Target [28].

The designed HIL testbed allows for testing the helicopter not only in hover but also in any smooth trajectories, such the cruise flight, figure-8, etc.

III. Testbed Modeling

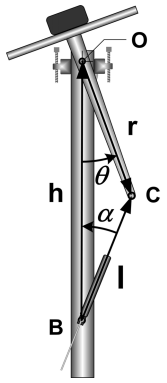

Fig. 4. Testbed mechanism

Using the Newton-Euler equations of motion, the attitude dynamic model of the helicopter and the testbed can be

written as

$$\dot{\vec{\omega}} = (\boldsymbol{I}+\boldsymbol{I_{tb}})^{-1}(\vec{\mathbf{M}}-\vec{\mathbf{M}}_{\mathbf{tb}})- \\ -(\boldsymbol{I}+\boldsymbol{I_{tb}})^{-1}(\vec{\omega}\times(\boldsymbol{I}+\boldsymbol{I_{tb}})\vec{\omega}) \quad (1)$$

where, the angular velocity of the helicopter in the body coordinates is denoted by $\vec{\omega} = [p\ q\ r]^T$, and $\boldsymbol{I}$ and $\boldsymbol{I_{tb}}$ are the moment of inertia tensors of the helicopter and the testbed, respectively. The moment of inertia due to the components on the testbed that are moving with the helicopter is almost ten times smaller that of the helicopter in pitch and five times smaller in roll, thus can be neglected. $\vec{\mathbf{M}}$ is the total moment vector applied to the helicopter from the main and tail rotor blades. The parasitic moment vector applied from the testbed to the helicopter is denoted by $\vec{\mathbf{M}}_{\mathbf{tb}}$, which is due to the damping effect of the cylinder, and its magnitude can be written as

$$M_{tb} = rb\dot{\ell}\cos(\frac{\pi}{2}-\theta-\alpha) \\ = rb\dot{\ell}\sin(\theta+\alpha) \quad (2)$$

where, b is the damping coefficient of the cylinder. $\dot{\ell}$ is the rate at which the cylinder elongates or shortens and can be calculated by taking time derivative of the loop closure equation in the complex plane for the planar mechanism "OBC". The following vector relation holds for the mechanism shown in Fig. 4

$$\vec{\mathbf{l}}-\vec{\mathbf{r}} = \vec{\mathbf{h}} \quad (3)$$

The loop closure equation can be written in the complex plane as

$$\ell\ e^{j(\frac{\pi}{2}-\alpha)} - r\ e^{-j(\frac{\pi}{2}-\theta)} = jh \quad (4)$$

Using Euler's formula results in

$$\ell(\sin(\alpha)+j\cos(\alpha)) - r(\sin(\theta)-j\cos(\theta)) = jh \quad (5)$$

Rearranging (5) results in

$$\ell\sin(\alpha) - r\sin(\theta) = 0 \quad (6)$$

$$\ell\cos(\alpha) + r\cos(\theta) = h \quad (7)$$

The testbed is designed to test the helicopter around hover, where the angles θ and α are small. Therefore, by rearranging (6) and (7) and assuming small angles results in

$$\ell\alpha - r\theta = 0 \quad (8)$$

$$\ell + r = h \quad (9)$$

Also, by differentiating from (6) and (7) with respect to time and assuming small angles results in

$$\dot{\ell}\alpha + \ell\dot{\alpha} - r\dot{\theta} = 0 \quad (10)$$

$$\dot{\ell} - \ell\alpha\dot{\alpha} - r\theta\dot{\theta} = 0 \quad (11)$$

Using (8) to (11) the equations are:

$$\alpha = \frac{r\theta}{h-r} \quad (12)$$

$$\dot{\ell} = r\dot{\theta}\frac{(\alpha+\theta)}{1+\alpha^2} \quad (13)$$

Since, α is small around hover, (13) can be simplified as

$$\dot{\ell} = r\dot{\theta}(\alpha+\theta) \quad (14)$$

Substituting (12) and (14) into (2) results in a parasitic testbed moment of

$$M_{tb} = \frac{h^2r^2}{(h-r)^2}b\theta^2\dot{\theta} \quad (15)$$

Therefore, the damping moment generated by the cylinder around hover is negligible (θ is small). However, if the helicopter on the testbed becomes unstable, it starts deviating from hover and the damping moment given in (15) will be no longer negligible but increases in a nonlinear manner. This prevents the helicopter from abrupt motion or hitting the hard end stoppers. With a negligible parasitic moment, M_{tb}, for small θ the testbed emulates hover condition and allows for the safe testing of the controller.

IV. Control Design

The control algorithm used in this paper is based on the Sliding Mode Control (SMC), which is robust to external disturbances. The sliding mode control design method in this section follows [29]. By writing the dynamic model of the helicopter in the following input-output control-affine form,

$$\ddot{\boldsymbol{y}}_{4\times1} = \boldsymbol{f}(\boldsymbol{y},\dot{\boldsymbol{y}})_{4\times1} + \boldsymbol{b}(\boldsymbol{y},\dot{\boldsymbol{y}})_{4\times4}\boldsymbol{u}_{4\times1} \quad (16)$$

where $\boldsymbol{f}(\boldsymbol{x})$ includes the nonlinear centrifugal and coriolis terms, $\boldsymbol{b}(\boldsymbol{x})$ is the control gain matrix, $\boldsymbol{u} = [\delta_{lon}, \delta_{lat}, \delta_{col}, \delta_{ped}]^T$ is the control input, and $\boldsymbol{y} = [x_{cp}, y_{cp}, z_{cp}, \psi_{cp}]^T$ is the control output and includes the 3D position of a point on the main hub axis above the CG, together with the heading of the helicopter. Since helicopters have two underactuated DOFs, as they are 6-DOF systems controlled by only four control inputs, a point on the main hub axis other than the CG is chosen as the point of control. Therefore, any deviations from the desired attitude would result in the deviation of the control point from its desired position [30]. This point is called the "Control Point (CP)". In general, a controller designed based on this approach controls the 3D position of the control point together with the heading of the helicopter.

To design a sliding controller, four asymptotically stable equations in the state-space $\boldsymbol{R}^{(2)}$ are defined,

$$\boldsymbol{s} = \dot{\boldsymbol{e}} + \boldsymbol{\lambda}\ \boldsymbol{e} = \boldsymbol{0} \quad (17)$$

where $\boldsymbol{s}$ is the surface function, $\boldsymbol{e} = \boldsymbol{y} - \boldsymbol{y^d}$ is the error of the control output from its desired value, and $\boldsymbol{\lambda} = diag(\lambda_1, \lambda_2, \lambda_3, \lambda_4)$, with all the components to be strictly positive, is the convergence rate. Rewriting (17) in the following form,

$$\boldsymbol{s} = \dot{\boldsymbol{y}} - \boldsymbol{s_r} \quad (18)$$

where $\boldsymbol{s_r} = \dot{\boldsymbol{y}}^d - \boldsymbol{\lambda e}$. Since, the surface defined by (17) is asymptotically stable, if the system is controlled such that $\boldsymbol{s}$ reaches zero and stays at zero at all times, the output error $\boldsymbol{e}$, will converge to zero. In order for $\boldsymbol{s}$ to be zero, the following

Lyapunov candidate function is defined,

$$V = \frac{1}{2}\boldsymbol{s}^T\boldsymbol{s} \tag{19}$$

In order for $\dot{V} \leq 0$, the control input is calculated as,

$$\boldsymbol{u} = \hat{\boldsymbol{b}}^{-1}(-\hat{\boldsymbol{f}} + \dot{\boldsymbol{s}}_{\boldsymbol{r}} - \boldsymbol{K}\ sat(\boldsymbol{\Phi}^{-1}\boldsymbol{s})) \tag{20}$$

where $\boldsymbol{K} = diag(k_1, k_2, k_3, k_4)$ is the sliding mode control gain matrix, and $\hat{\boldsymbol{b}}$ and $\hat{\boldsymbol{f}}$ are the system matrices calculated using nominal values of the model parameters. To avoid chattering a continuous saturation function with the boundary layer thickness $\boldsymbol{\Phi}$ is used in (20).

In the absence of any model mismatch and uncertainties in (16), selection of any positive definite matrix $\boldsymbol{K}$ in (20) would result in the convergence of the error $\boldsymbol{e}$ to zero. The presence of external disturbances or parameter uncertainties necessitates the components of $\boldsymbol{K}$ to be large enough to satisfy the following sliding condition,

$$\dot{V} \leq -\boldsymbol{\eta}|\boldsymbol{s}| \tag{21}$$

where $\boldsymbol{\eta}$ has strictly positive components, and determines the convergence rate to the surface. This condition results in the following formula for the sliding control gain,

$$\begin{aligned}(1-\Delta_{ii})k_i \quad &+ \quad \sum_{j\neq i}^{4}\Delta_{ij}k_j = F_i + \eta_i \\ &+ \quad \sum_{j=1}^{4}\Delta_{ij}|\dot{s}_{ri} - \hat{f}_j|, \quad i = 1,...,4\end{aligned} \tag{22}$$

where, $\boldsymbol{F}$ and $\boldsymbol{\Delta}$ are the uncertainty bound matrices as,

$$|\boldsymbol{f} - \hat{\boldsymbol{f}}| \leq \boldsymbol{F} \tag{23}$$

$$\boldsymbol{b} = (\mathbf{I}_{4\times 4} + \boldsymbol{\delta})\hat{\boldsymbol{b}}, \quad |\boldsymbol{\delta}| \leq \boldsymbol{\Delta} \tag{24}$$

By knowing the uncertainty bounds $\boldsymbol{F}$ and $\boldsymbol{\Delta}$, and calculating (22) at each sampling time, it is guaranteed that the control outputs will follow their desired trajectories.

V. Experimental Results

The airframe to be tested in this work is the Evolution Ex shown in Fig. 5, which is an electric model helicopter with a $2m$ blade span and payload of $10kg$. The Avionics of the helicopter is shown in Fig. 6 and includes: a PC-104 microcomputer as the real-time embedded controller, a Crossbow NAV440 GPS-Aided Inertial Measurement Unit (IMU), an Xstream RF modem for communicating with the ground station, a Servo Switch Card (SSC) for switching between the radio and automatic control, and a microcontroller for the battery voltage and current monitoring.

The ground station computer communicates with the Avionics on the helicopter using a pair of RF modem receivers and allows for online updating and uploading the control gains as well as monitoring the attitude, rotor speed, and voltage and current of the batteries. The communication interface of the ground station is shown in Fig. 7.

Fig. 5. Evolution EX helicopter

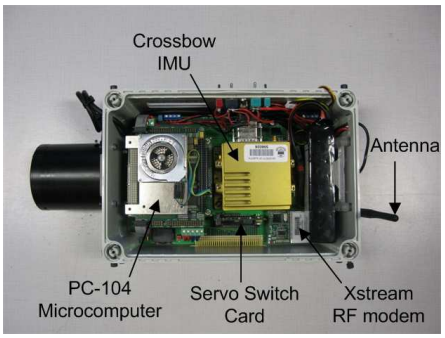

Fig. 6. Avionics of the helicopter

A. Longitudinal Control Experiment

The longitudinal control of the helicopter is tested by placing the vehicle on the testbed as shown in Fig. 8. Only the longitudinal motion of the helicopter is tested in this experiment, so the physical rotation around the vertical axis of the testbed is restricted mechanically. Although, the helicopter is physically allowed to rotate only around the pitch axis in this experiment, the controller is controlling all 6-DOFs of the helicopter. The actual motion of the helicopter is calculated using the 6-DOF nonlinear model of the helicopter at every sampling time as described in Fig. 3.

The CG of the helicopter shown in Fig. 8 is aligned with the axis of rotation. Depending on the size of the blades and the maximum rolling and pitching moments generated, the needle valve on the damping cylinder shown in Fig. 2 is adjusted. To emulate hover, a constant collective pitch at hover of $\delta_{col} = 5.6deg$ for Evolution EX, is used throughout this experiment. After the main rotor reached the nominal spinning speed of $1100rpm$ and the collective pitch at hover, the automatic control is activated using the Servo Switch Card (SSC) module on the Avionics, and the onboard controller takes over to stabilize the helicopter. The control results for the longitudinal motion are shown in Figs. 9 and 10.

The Control Point (CP) is chosen to be $3m$ above the CG on the main hub axis for the Evolution EX helicopter. Although, the Control Point approach, described in section IV, is used in this paper to tune the gains of the Sliding Mode controller, the testbed can be used for tuning any controller designed using any approach.

The damping mechanism prevents the helicopter from

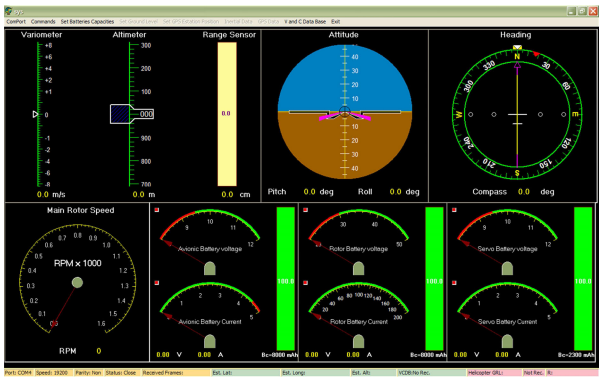

Fig. 7. Ground station interface

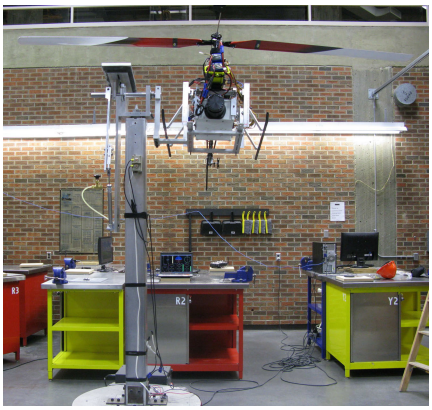

Fig. 8. HIL testbed setup for the pitch control in hover

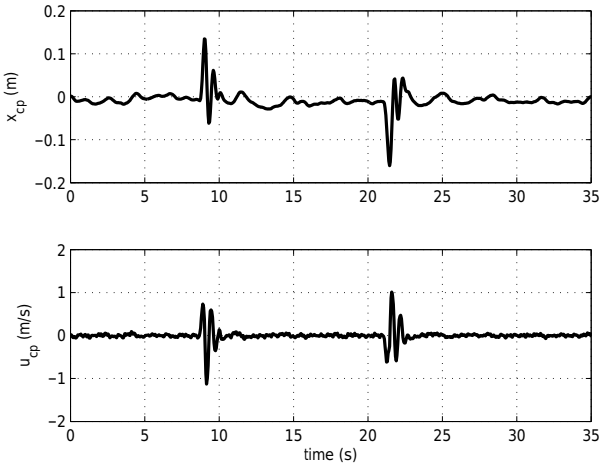

Fig. 9. Position and velocity of the control point in the longitudinal control - the two overshoots at 8.5 and 21 seconds are due to the external disturbances

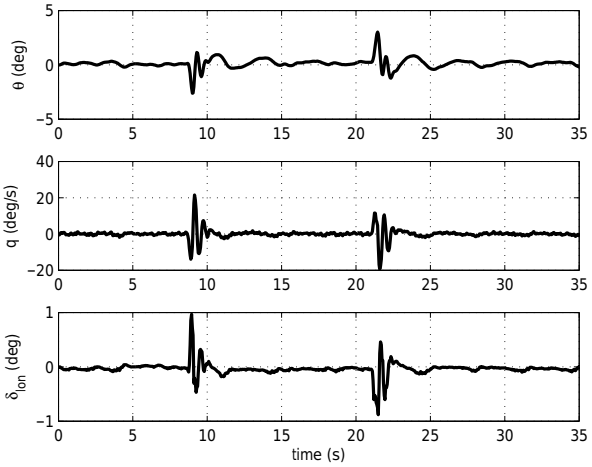

Fig. 10. Closed-loop pitch response and longitudinal cyclic input in the presence of external disturbances

sudden movements that can cause damage to the vehicle, and smoothly slows down its motion which allows for testing the controller as many times as required until the gains are tuned and the desired response is achieved. Then once the desired gains are set, the damping effect can be reduced by adjusting the needle valve or by removing the cylinder so that controller is tested freely against the imposed external disturbances. The closed-loop responses of the control point position and velocity along the longitudinal axis are shown in Fig. 9, and the pitch angle, pitch rate, and the longitudinal cyclic command are shown in Fig. 10. During the experiment the helicopter was disturbed two separate times at 8.5 and 21 seconds, by manually exerting a moment of about $2.5N.m$ to the fuselage for about 1 second to tilt it away from the level position. As shown in Figs. 9 and 10, the controller actuates the longitudinal cyclic pitch of the main rotor blades to reject the disturbances and maintain the zero position and velocity of the control point along the longitudinal axis to within $\pm 2cm$ and $\pm 4cm/s$, respectively. Also, the steady state pitch angle and pitch rate are close to zero, which show that the controller stabilizes the longitudinal motion of the helicopter in the presence of the external disturbances.

B. *Lateral Control Experiment*

The lateral control of the helicopter is tested by securing it on the testbed as shown in Fig. 11. In this position, the CG of the helicopter is aligned with the axis of rotation as in the side view of Fig. 2. Similar to the previous test, once the main rotor reached the nominal speed of about $1100rpm$ and the collective pitch of $5.6deg$ at hover, the controller is switched on for lateral control of the helicopter.

The closed-loop response of the control point position and velocity along the lateral axis is shown in Fig. 12, while the roll angle, roll rate, and the lateral cyclic command are shown in Fig. 13. During the experiment the helicopter is manually disturbed three times at 7, 13 and 19 seconds, by applying a moment of about $2.5N.m$ to the fuselage for approximately 1 second to tilt it away from its desired position in hover. This test demonstrates that the controller adjusts the lateral cyclic pitch of the main rotor blades to reject the disturbances

Fig. 11. HIL testbed setup for the roll control in hover

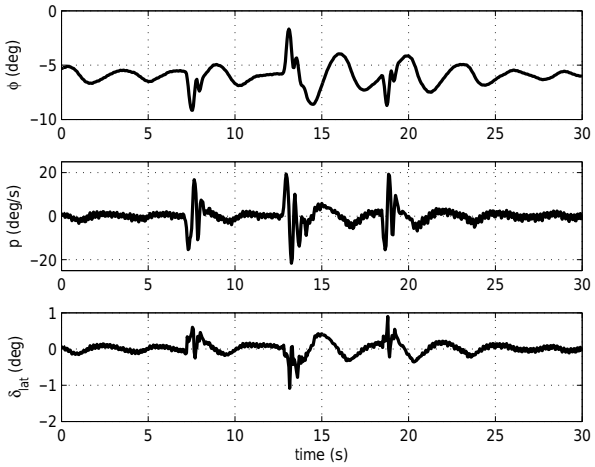

Fig. 13. Closed-loop roll response and lateral cyclic input in the presence of external disturbances

and maintain the zero position and velocity of the control point along the lateral axis to within $\pm 2cm$ and $\pm 8cm/s$, respectively. The results in Fig. 13 show that the desired steady state roll angle is not zero and is about $-6deg$. This is due to the fact that in hover, the helicopter must have a slight bank angle to compensate for the tail rotor thrust, and the desired steady state roll rate is zero which shows that the controller stabilizes the lateral motion of the helicopter in the presence of disturbances.

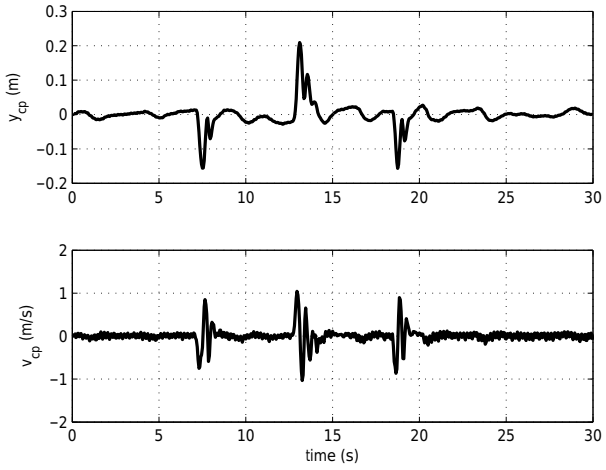

Fig. 12. Position and velocity of the control point in the lateral control - the three overshoots at 7, 13 and 19 seconds are due to the external disturbances

C. Heading Control Experiment

To test the heading control, the helicopter is mounted on the HIL testbed shown in Fig. 14, with the arm set removed and a flat aluminum plate attached on top of the U-shape plate. The Helicopter is then mounted on the flat plate such that its CG is aligned with the vertical axis of the pole as shown in the schematic in Fig. 15. Similar to the previous tests, a constant collective pitch at hover of $\delta_{col} = 5.6deg$ is maintained after the main blades reached the nominal spinning speed of $1100rpm$. Then, the automatic control is activated to control the yaw motion of the helicopter to the desired trajectory.

Fig. 14. HIL testbed setup for the yaw control

Both a step and a figure-8 yaw trajectory are tested with the results shown in Figs. 16 and 17, respectively. Figure 16 shows the yaw angle, yaw rate, and tail command in the yaw control of a fast step trajectory. The results demonstrate that the controller maintains the desired yaw angle and yaw rate with an accuracy of $\pm 1deg$ and $\pm 0.5deg/s$, respectively.

In Fig. 17, during the figure-8 trajectory experiment the helicopter is subject to a large disturbance for the period of 60-80 seconds. This is done by manually deviating the fuselage away from the desired trajectory. The results in Fig. 17 show that the controller actuates the pitch of the tail rotor blades to reject the disturbance and maintain the desired yaw angle and yaw rate within $\pm 1deg$ and $\pm 0.7deg/s$,

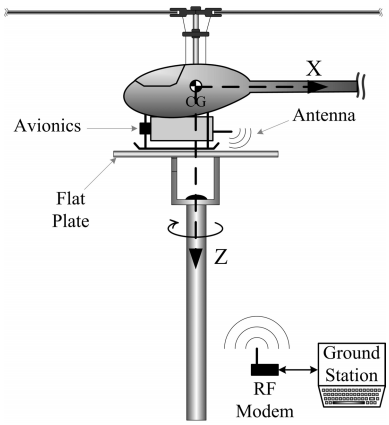

Fig. 15. HIL Testbed schematic for the heading experiment

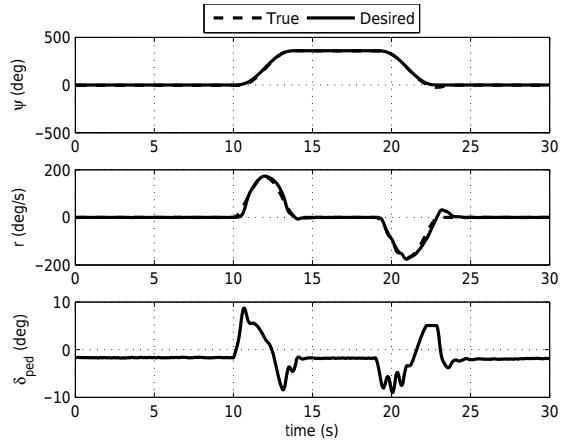

Fig. 16. Closed-loop yaw response to the step trajectory

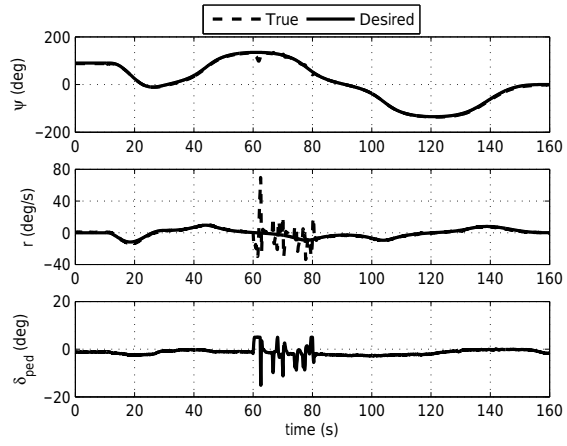

Fig. 17. Closed-loop yaw response to the figure-8 trajectory - the overshoot at about 60 seconds is due to the external disturbance applied to the helicopter fuselage at 60 seconds

respectively.

The control parameters for the longitudinal, lateral, and heading motion, obtained from the HIL experiments, are listed in Table I.

TABLE I

CONTROL PARAMETERS OBTAINED FROM THE HIL EXPERIMENTS

Parameter	Description	Longitudinal	Lateral	Heading
λ	*Convergence rate*	2.5	2.5	2.5
F	*Bound on f*	10	15	1
Δ	*Bound on b*	0.5	0.5	0.5
η	*Surface reach time*	1	1	1
Φ	*Boundary layer THK*	0.8	0.6	1

VI. CONCLUSIONS

In this paper, a HIL testbed for testing small unmanned helicopters on the ground has been described. The testbed provides a safe and low-cost platform to implement a control algorithm and tune the control gains, as well as to test the robustness of the controller against external disturbances in a controlled environment. A 6-DOF mathematical model of the helicopter is needed to determine the actual motion of the helicopter in the HIL system. A mathematical modeling of the testbed is also developed in this paper. A small unmanned helicopter is tested on the testbed in three seperate experimental tests. The three tests performed for longitudinal, lateral, and heading control. The experimental results showed that the controller designed using the HIL testbed achieved a $\pm 2cm$ accuracy on the longitudinal and lateral position tracking, and a $\pm 1deg$ accuracy on the heading trajectory tracking in the presence of external disturbances.

REFERENCES

[1] L. Merino, F. Caballero, J. Martnez-de Dios, I. Maza, and A. Ollero, "An unmanned aircraft system for automatic forest fire monitoring and measurement," *J Intell Robot Syst*, vol. 65, pp. 533–548, 2012.

[2] D. Casbeer, R. Beard, T. McLain, S.-M. Li, and R. Mehra, "Forest fire monitoring with multiple small UAVs," in *ACC*, June 2005, pp. 3530 – 3535 vol. 5.

[3] Z. Li, Y. Liu, R. A. Walker, R. F. Hayward, and J. Zhang, "Towards automatic power line detection for a UAV surveillance system using pulse coupled neural filter and an improved hough transform," *Machine Vision and Applications*, vol. 21, no. 5, pp. 677–686, September 2009.

[4] C. A. Marinho, C. de Souza, T. Motomura, and A. G. da Silva, "In-service flare inspection by unmanned aerial vehicles (UAVs)," in *18th World Conference on Nondestructive Testing*, Durban, South Africa, April 2012.

[5] R. Haarbrink and H. Eisenbeiss, "Accurate DSM production from unmanned helicopter systems," *Int. Arch. Photogramm. Remote Sens. Spat. Inf. Sci*, vol. 37, pp. 1259–1264, 2008.

[6] J. Gundlach, *Designing Unmanned Aircaft Systems: A comprehensive Approach*, 1st ed. 1801 Alexander Bell Drive, Reston, Virginia 20191-4344, USA: American Istitute of Aeronautics and Astronautics, Inc, 2012.

[7] Y. Zhang, A. Chamseddine, C. Rabbath, B. Gordon, C.-Y. Su, S. Rakheja, C. Fulford, J. Apkarian, and P. Gosselin, "Development of advanced FDD and FTC, techniques with application to an unmanned quadrotor helicopter testbed," *J. Franklin Inst.*, 2013.

[8] W. Green and P. Oh, "Autonomous hovering of a fixed-wing micro air vehicle," in *ICRA*, May 2006, pp. 2164 –2169.

[9] H. Oh, D.-Y. Won, S.-S. Huh, D. Shim, M.-J. Tahk, and A. Tsourdos, "Indoor UAV control using multi-camera visual feedback," *J Intell Robot Syst*, vol. 61, pp. 57–84, 2011.

[10] L. Garca Carrillo, E. Rondon, A. Sanchez, A. Dzul, and R. Lozano, "Stabilization and trajectory tracking of a quad-rotor using vision," *J Intell Robot Syst*, vol. 61, pp. 103–118, 2011.
[11] I. Mellado-Bataller, J. Pestana, M. Olivares-Mendez, P. Campoy, and L. Mejias, "MAVwork: A framework for unified interfacing between micro aerial vehicles and visual controllers," in *Frontiers of Intelligent Autonomous Systems*, ser. Studies in Computational Intelligence. Springer Berlin Heidelberg, 2013, vol. 466, pp. 165–179.
[12] A. Chamseddine, Y. Zhang, C. Rabbath, C. Join, and D. Theilliol, "Flatness-based trajectory planning/replanning for a quadrotor unmanned aerial vehicle," *IEEE Transactions on Aerospace and Electronic Systems*, vol. 48, no. 4, pp. 2832 –2848, October 2012.
[13] H. Chao, Y. Cao, and Y. Chen, "Autopilots for small unmanned aerial vehicles: A survey," *International Journal of Control, Automation and Systems*, vol. 8, pp. 36–44, 2010.
[14] C. Guowei, W. Biao, B. Chen, and T. Lee, "Design and implementation of a flight control system for an unmanned rotorcraft using RPT control approach," in *30th Chinese Control Conference (CCC)*, July 2011, pp. 6492 –6497.
[15] C. Castillo, W. Moreno, and K. Valavanis, "Unmanned helicopter waypoint trajectory tracking using model predictive control," in *Mediterranean Conference on Control Automation*, June 2007, pp. 1 –8.
[16] R. D. Garcia and K. P. Valavanis, "The implementation of an autonomous helicopter testbed," *J Intell Robotics Syst*, vol. 54, no. 1-3, pp. 423–454, Mar. 2009.
[17] H. Kim and D. H. Shim, "A flight control system for aerial robots: algorithms and experiments," *Control Engineering Practice*, vol. 11, no. 12, pp. 1389 – 1400, 2003.
[18] S. P. Khaligh, F. Fahimi, and M. Saffarian, "Comprehensive aerodynamic modeling of a small autonomous helicopter rotor at all flight regimes," in *AIAA Modeling and Simulation Technologies Conference*, Chicago, Illinois, United States, 2009, pp. 1 – 10.
[19] K. Tanaka, H. Ohtake, and H. O. Wang, "A practical approach to stabilization of a 3-DOF RC helicopter," *IEEE CONTROL SYST TECHNOL*, vol. 12, no. 2, pp. 315–325, March 2004.
[20] A. T. Kutay, A. J. Calise, M. Idan, and N. Hovakimyan, "Experimental results on adaptive output feedback control using a laboratory model helicopter," *IEEE CONTROL SYST TECHNOL*, vol. 13, no. 2, pp. 196–202, March 2005.
[21] B. Andrievsky, D. Peaucelle, and A. L. Fradkov, "Adaptive control of 3-DOF motion for LAAS helicopters benchmark: Design and experiments," in *ACC*, July 2007, pp. 3312–3317.
[22] Q. C. Inc., 2013. [Online]. Available: http://www.quanser.com
[23] J. F. Montgomery, A. E. Johnson, S. I. Romeliotis, and L. H. Matthies, "The jet propulsion laboratory autonomous helicopter testbed: A platform for planetary exploration technology research and development," *Journal of Field Robotiics*, vol. 23, no. 3/4, pp. 245–267, 2006.
[24] N. Vitzilaios and N. Tsourveloudis, "An experimental test bed for small unmanned helicopters," *J Intell Robot Syst*, vol. 54, pp. 769–794, 2009.
[25] R. Whitman, "Training apparatus for remote control model helicopters," U.S. patent US4 917 610, 1990.
[26] M. F. Weilenmann and H. P. Geering, "Test bench for rotorcraft hover control," *J GUID CONTROL DYNAM*, vol. 17, no. 4, pp. 729 – 736, 1994.
[27] V. Narli and P. y. Oh, "A hardware-in-the-loop test rig for desining near-earth aerial robotics," in *Proceedings of the 2006 IEEE International Conference on Robotics and Automation*, 2006.
[28] I. The MathWorks, 2013. [Online]. Available: http://www.mathworks.com/
[29] J. J. E. Slotine and L. Weiping, *Applied Nonlinear Control*. Englewood Cliffs, NJ: Prentice-Hall, Inc., 1991.
[30] F. Fahimi and M. Saffarian, "The control point concept for nonlinear trajectory-tracking control of autonomous helicopters with fly-bar," *International Journal of Control*, vol. 84, no. 2, pp. 242 – 253, 2011.